DALTON
FULL PAPER

Spectroelectrochemical investigation of a dinuclear cobalt porphyrin complex with ionic groups in DMSO †

Kimihisa Yamamoto,* Shinsuke Nakazawa, Akiko Matsufuji and Takeyoshi Taguchi

Department of Chemistry, Faculty of Science & Technology, Keio University, Yokohama 223-8522, Japan. E-mail: yamamoto@chem.keio.ac.jp

Received 14th August 2000, Accepted 5th December 2000
First published as an Advance Article on the web 15th January 2001

The dinuclear cobalt porphyrin of (5,10,15,20-tetrakis(*N*-methyl-4-pyridinio)porphyrinato)cobalt(II) (CoTMPyP) with (5,10,15,20-tetrakis(4-sulfonatophenyl)porphyrinato)cobaltate(II) (CoTPPS) has allowed spectroelectrochemical analysis of electron transfer processes in DMSO. In the II–II valence state it undergoes stepwise two-electron transfer accompanied by a dissociation equilibrium ($K_d = 1.3 \times 10^{-6}$ M) with redox potentials at −0.37 and −0.17 V *vs.* $Fc–Fc^+$. The kinetics of the dissociation allows a snapshot of the species present without perturbing the equilibrium distribution. The dissociation in the II–II valence state is promoted by oxidation to the higher valence states due to the increasing charge on the complex and solvation of DMSO at the cobalt. The dissociation constants of the dinuclear porphyrin in the II–III and III–III valence states were determined to be 2.5×10^{-6} and 5.0×10^{-6} M, respectively, using Job plots. EXAFS analysis reveals that the Co · · · Co distance in the dimeric porphyrins is 3.37 Å which is not drastically influenced by the valence state in the solid state. The dinuclear cobalt porphyrin complex acts as an excellent catalyst for reduction of oxygen in which the number of electrons transferred was determined to be $n = 3.9$ based on Koutecky–Levich plots.

Introduction

The self-assembling or multinuclear porphyrins have attracted significant attention in inorganic chemistry because biologically active porphyrins usually occur as dimers in solution [1] and protein matrices, *e.g.* the "special pair" of chlorophylls in solution and photosynthetic reaction centers, and the diamagnetic dimers of metalloporphyrin cation radicals in solution.[2] In humans, the breath enzyme, cytochrome oxidase, dominates the 4-electron reduction of oxygen to water under atmospheric pressure in the multi-nuclear center. Many researchers have spent considerable effort on structural analysis of the enzyme [3,4] and mimicking its catalytic reactions.[5–8] Research on the breath reaction, the 4-electron reduction of oxygen to water, is important in order not only to determine its mechanism but also to make novel catalysts.[9–15] Multinuclear porphyrins such as dimeric porphyrins, tetraruthenated porphyrin, and polymeric porphyrins have been employed as catalysts for 4-electron reduction of oxygen. The dimeric cobalt porphyrins [16,17] preferentially act as the catalyst.

Therefore, numerous studies have involved spectroscopic analysis of ionically assembling metallo-porphyrins or metal-free porphyrins.[18–22] Aggregation is promoted in the metal-free porphyrin in water due to its hydrophobicity and planarity even under ultra-dilute conditions. The poor solubility makes it difficult to analyse homogeneously the electron transfer process. We found that the ionically dimeric cobalt porphyrins are soluble in dimethyl sulfoxide (DMSO) due to its weak coordination ability towards cobalt, which allowed us to perform electrochemical measurements. This paper reports the electron transfer process of an ionically dimeric cobalt porphyrin accompanied by a dissociation process. Our results reveal that the 4-electron reduction of oxygen can be achieved with high stability using a polyaniline cobalt(II) porphyrin catalyst.

On the other hand, since the dimeric porphyrin has a π-space between the two metal centers with a short distance as a characteristic structure, it is also very interesting to know whether or not the two metal centers electrochemically interact with each other in the mixed valence state($Co^{II}–Co^{III}$).[23–27] The ionically dimeric cobalt porphyrin is a good model for elucidating interaction through space or a π–π stacking orbital between each porphyrin ring because the cobalt porphyrins are strongly attracted to each other by the 4 ionic groups on each.

Experimental

Reagents

Regent grade DMSO and CoTPP used as a solvent were from the Kantoh Chemical Company, Inc., tetrabutylammonium perchlorate and KPF_6 used as the supporting electrolyte after recystallization from Tokyo Kasei Co.

Syntheses (see ESI supplementary information)

(5,10,15,20-Tetrakis(*N*-methyl-4-pyridinio)porphyrinato)-cobalt(II). 5,10,15,20-Tetrakis(*N*-methyl-4-pyridinio)porphyrin free base (H_2TMPyP) was purchased from Tokyo Kasei Inc. as a toluenesulfonate salt. (5,10,15,20-Tetrakis(*N*-methyl-4-pyridinio)porphyrinato)cobalt(II) (CoTMPyP) was synthesized as described previously.[28] The purity of the tetra-*p*-toluenesulfonate salt was confirmed by comparison of the spectrum with those previously reported [29,30] (see ESI supplementary data). The product was isolated in 68% yield by drying *in vacuo* for 12 h. UV-vis(DMSO) λ/nm, (ε/M^{-1} cm^{-1}) 428(1.57×10^5) and 536 (0.17×10^5). Co(III)TMPyP was synthesized by air oxidation in hydrochloric acid. After precipitation in acetone it was dried *in vacuo* for 12 h. The crude product was purified using anion exchange (Amberlite GC400, chloride form). The product was isolated after drying *in vacuo* for 12 h. UV-vis(DMSO): λ/nm (ε/M^{-1} cm^{-1}) 441 (1.59×10^5) and 553 (0.18×10^5).

† Electronic supplementary information (ESI) available: detailed experimental procedures and characterization data of cobalt porphyrins, and detailed derivation of the kinetic equation. See http://www.rsc.org/suppdata/dt/b0/b006619m/

DOI: 10.1039/b006619m

Tetrasodium (5,10,15,20-tetrakis(4-sulfonatophenyl)porphyrinato)cobalt(II). The free base 5,10,15,20-tetrakis(4-sulfonatophenyl)porphyrin(H_2TPPS) was purchased from Tokyo Kasei Inc. The synthesis of tetrasodium (5,10,15,20-tetrakis(4-sulfonatophenyl)porphyrinato)cobaltate(II) (CoTPPS) was performed as previously.[31] The spectrum of the product agreed with those previously reported[32–33] (see ESI supplementary data). The product was isolated in 90% yield after drying *in vacuo* for 12 h. UV-vis(DMSO): λ/nm (ε/M^{-1} cm^{-1}) 416 (1.96×10^5) and 533 (0.15×10^5). Co(III)TPPS was synthesized by air oxidation in hydrochloric acid. After precipitation in acetone it was died *in vacuo* for 12 h. The crude product was purified through cation exchange (Amberlite GC120, Na^+ form). The product was isolated in 76% yield after drying *in vacuo* for 12 h. UV-vis(DMSO): λ/nm, ε/M^{-1} cm^{-1}) 435 (2.85×10^5) and 548 (0.18×10^5).

Spectroscopic measurements

The UV-vis spectra were obtained using a Shimadzu UV-2400PC spectrometer with a quartz cell (optical path length: 1 cm). The titration was carried out by adding 2 mL of DMSO solution to the quartz cell using a micro-syringe. Near infrared spectra were measured using a JASCO Co. V-570 spectrometer, ^{1}H and ^{13}C NMR spectra on a JEOL 400-MHz FT-NMR JMN400 and IR spectra using a Shimadzu FT-IR 8300 spectrometer and potassium bromide pellets.

Electrochemical measurements

The electrochemical analysis was performed using an electrochemical work station (BAS Co. Ltd., Model 660) under the following conditions. Cyclic voltammetry was carried out in a conventional two-compartment cell under an N_2 atmosphere after N_2 bubbling for 30 min. A platinum disk electrode was used as the working electrode and polished with 0.05 mm alumina paste before the experiments. The auxiliary electrode was a coiled platinum wire separated from the working electrode by a fine-porosity frit. The reference electrode was Ag–Ag^+. The formal potential was normalized to the ferrocene–ferrocenium couple in acetonitrile. The scanning rate was 100–10 mV s^{-1}. Rotating disk voltammetry was carried out using the same instruments. The rotating rate was 200–1000 rpm. Spectroelectrochemistry was carried out using the same equipment. The cell was prepared by placing a Teflon sealing tape between the ITO electrode and the glass plate. The optical path length was estimated to be *ca*. 6.5 μm.

EXAFS measurement

An EXAFS analysis was carried out using a Rigaku R-EXAFS 2000 instrument (filament, LaB_6, target, Mo; detector, proportional counter), based on the single crystal transmission method. The cobalt K-edge spectra were measured by scanning with high-energy resolution using a Ge(400) crystal. Data reduction followed conventional edge normalization, extraction of the EXAFS signal $\chi(k)$ and its Fourier transformation. Curve fitting calculations were performed to determine the coordination number, atom distance, and edge shift without restriction using a fixed Debye–Waller factor (0.06) and mean free path (7).

Oxygen reduction

2,3-Dicarboxyaniline in anionic state was oxidatively polymerized in aqueous solution by $Na_2S_2O_8$ as an oxidant to yield poly(2,3-dicarboxyaniline), the preparation of which was reported previously.[34] The resulting polyaniline was used as a conductive matrix for the cobalt porphyrin polymer complex, acting as an excellent electron mediator due to matching of its redox potential with that of the cobalt porphyrin. Co(II)TPPS and Co(II)TMPyP immediately aggregated to precipitate a powder after mixing in methanol due to the hydrophobicity of the dinuclear porphyrin. The precipitate is soluble in DMSO below a 0.1 mM concentration. The formation of the dinuclear porphyrin in DMSO is supported by previous results.[35,36] The catalytic behavior of the polyaniline–CoTMPPy-CoTPPS complex (PAn-Co2P) was studied using cyclic voltammetry at a modified glassy carbon electrode. Poly(2,3-dicarboxyaniline) as an emeraldine base (0.15 mM) and the dinuclear cobalt porphyrin (0.05 mM) were mixed in 10 mL of DMSO with a 3 : 1 molecular unit stoichiometry. A homogeneous polymer catalyst film of PAn-Co2P (Co2P: 1.77×10^{-9} mol cm^2) was prepared by casting on the electrode. Electrochemical measurements were carried out in 0.1 M KPF_6 aqueous solution (pH 6.15).

In case of the monomeric cobalt porphyrin, oxygen reduction was carried out at a glassy carbon electrode modified only by CoTPP (2.83×10^{-9} mol cm^{-2}) which was cast using chloroform solution. Rotating disk voltammograms were measured at 5 mV scanning rate in sodium acetate and acetic acid buffer solution(pH 4.5) which is the same pH as that of the PAn complex domain. The number of electrons transferred was determined to be 2 ± 0.2 from a Koutechy–Levich plot.

Koutechy–Levich equation

The Koutechy–Levich expression is as shown in eqn. (1) where

$$1/i_{lim} = (1/I_i) + (1/I_k) \quad (1)$$

$I_i = 0.62nFACD^{2/3}v^{-1/6}\omega^{1/2}$, $I_k = 10^3nkG\Gamma FC$, i_{lim} = limiting current (A), n = number of electrons transferred, F = Faraday constant = 96485 C mol^{-1}, A = area of electrode = 0.2827 cm^2, C = oxygen concentration = 0.28 mM, D = diffusion coefficient of oxygen = 1.7×10^{-5} cm^2 s^{-1}, v = dynamic viscosity of water = 0.01 cm s^{-1}, ω = rotation rate of the electrode (rad s^{-1}), Γ = surface concentration of catalyst (mol cm^{-2}) and k = rate constant (M^{-1} s^{-1}). The dashed lines in Fig. 9 (n = 2 or 4) were derived using the above parameters.

Kinetic analysis

The kinetics was analysed based on eqn. (2). The 2nd order

$$A + B \underset{k_b}{\overset{k_f}{\rightleftharpoons}} AB \quad (2)$$

kinetics of this equilibrium is given by eqns. (3)–(5) (see ESI Supplementary Information), where k_f, k_b are rate constants of the forward and back reaction, respectively, A_0 is the initial concentration of A, A_r is the absorbance in the reaction mixture, ε_A, ε_B, and ε_{AB} are molar absorption coefficients of A, B and AB, respectively.

$$k_f t = \frac{K}{\sqrt{1 + 4A_0K}} \ln \frac{-2A_0^2K + (2A_0K + 1 - \sqrt{1 + 4A_0K})x}{-2A_0^2K + (2A_0K + 1 + \sqrt{1 + 4A_0K})x} = F(x) \quad (3)$$

$$K_d^{-1} = K = k_f/k_b \quad (4)$$

$$x = [A_r - A_0(\varepsilon_A + \varepsilon_B)]/[\varepsilon_{AB} - (\varepsilon_A + \varepsilon_B)] \quad (5)$$

Results and discussion

Electrochemical and spectroscopic studies of monomeric cobalt porphyrins were performed in order to compare their properties with those of dinuclear porphyrin compounds. The reversible redox wave of CoTMPyP attributed to the Co^{II}–Co^{III} couple was observed at −0.21 V *vs.* Fc–Fc^+ during cyclic voltammetry (Fig. 1a). In contrast, CoTPPS did not show a

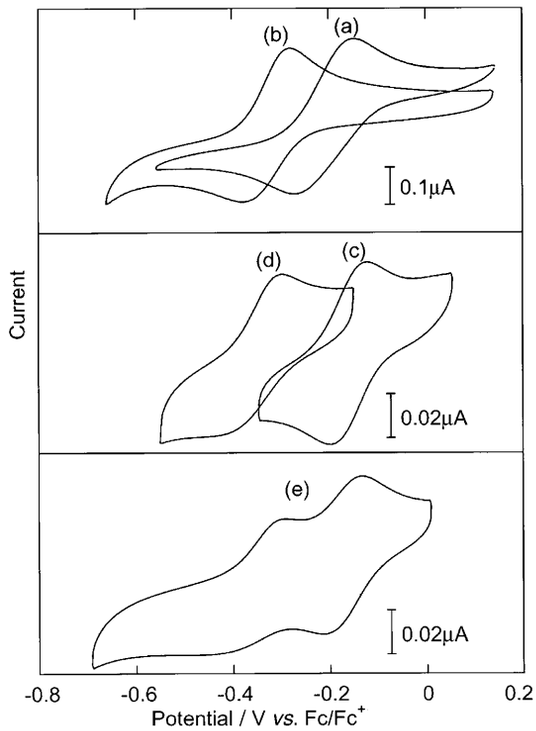

Fig. 1 Cyclic voltammograms of (a) 0.5 mM CoTMPyP in DMSO, (b) 0.5 mM of CoTPPS in the presence of 5 wt% trifluoroacetic acid in DMSO, (c) 0.1 mM H_2TPPS–CoTMPyP, (d) 0.1 mM CoTPPS-H_2TMPyP and (e) 0.1 mM CoTPPS-CoTMPyP. scan rate $v = 10$ mV s^{-1}, supporting electrolyte 0.05 M tetrabutylammonium perchlorate, potential adjusted using ferrocene (V *vs.* $Fc–Fc^+$).

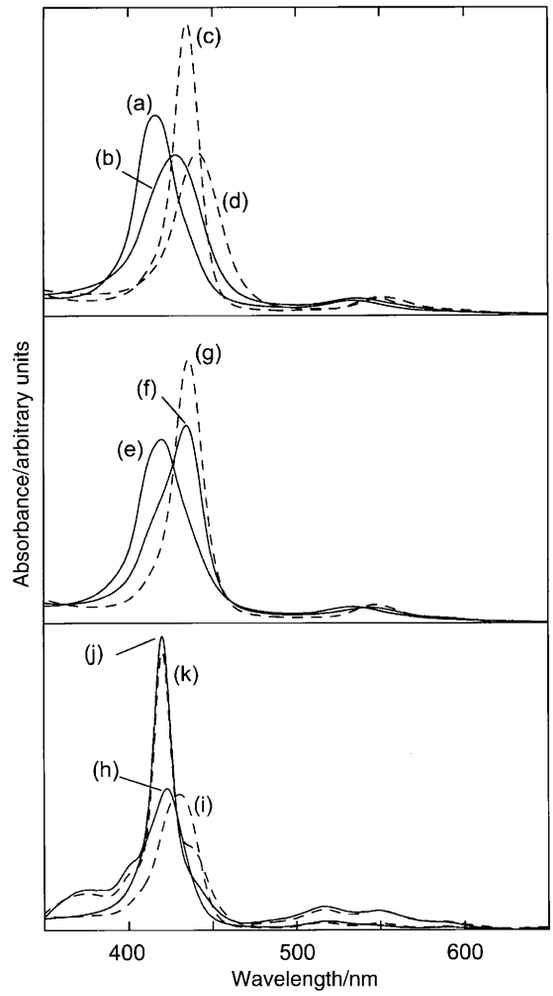

Fig. 2 UV-vis absorption spectra of cobalt porphyrins (0.5 mM) in DMSO obtained by spectroelectrochemical measurement: (a) Co(II)-TPPS, (b) Co(II)TMPyP, (c) Co(III)TPPS at 0.1 V applied potential, (d) Co(III)TMPyP at 0.1 V applied potential, (e) Co(II)TPPS–Co(II)TMPyP, (f) Co(III)TPPS–Co(II)TMPyP at −0.27 V applied potential, (g) Co(III)TPPS–Co(III)TMPyP at 0.1 V applied potential, (h) Co(II)TPPS–H_2TMPyP, (i) Co(III)TPPS–H_2TMPyP at 0.1 V applied potential, (j) H_2TPPS–Co(II)TMPyP, and (k) H_2TPPS–Co(III)TMPyP at 0.1 V applied potential.

good redox couple due to the slow coordination of DMSO during the oxidation. The redox activity is observed upon addition of *ca.* 5 wt% trifluoroacetic acid due to a change of the ligand, giving a redox potential at −0.33 V *vs.* $Fc–Fc^+$ (Fig. 1b).

Spectroelectrochemical measurements were performed in order to identify the redox couple as Co^{II}–Co^{III}. During the oxidation, the Soret and Q bands shifted to the long wavelength region with isosbestic points (Fig. 2a–2d). The characteristic Soret and Q bands appear at 441 and 553 nm, respectively, for Co(III)TMPyP. Co(III)TPPS shows these bands at 435 and 548 nm, respectively, even in the absence of trifluoroacetic acid. This result is caused by the longer timescale of the measurement than that of cyclic voltammetry. Thus the redox couple does not correspond to oxidation of the porphyrin ring but to Co^{II}–Co^{III}.[33,37,38]

The aggregation behavior of porphyrin complexes with ionic groups has been investigated by many researchers.[18–21,36,39] Aggregation of CoTPPS and CoTMPyP results in a precipitate in water or methanol which is not soluble in dichloromethane, chloroform, tetrahydrofuran and acetonitrile. The very weak coordination ability of water or methanol results in the formation of an oligomer and polymer of the cobalt porphyrins. We found that the precipitate shows a slight solubility in DMSO. The weak coordination ability towards the cobalt porphyrins prevents oligomerization of the aggregate. Titration by adding Co(II)TPPS to a Co(II)TMPyP solution was performed in order to analyse the aggregation dynamics. The results of the reverse titration of Co(II)TPPS by adding Co(II)TMPyP are shown in Fig. 3. The spectra changed with an isosbestic point in the region of the equivalence ratio 1:1. At this equivalence point the absorbance was lower than the sum of those of CoTPPS and CoTMPyP, which means that a chemical reaction takes place in the system. Only one isosbestic point during the titration indicates the formation of one species, the dinuclear porphyrin. The change in the absorbance is caused by overlapping of the π-electron clouds on the porphyrin rings.

Similar aggregation phenomena were observed in the system of metal-free porphyrin and the cobalt(III) porphyrins. On the basis of Job's method, a quantitative analysis was performed during the titration (Fig. 4)[40,41] using eqns. (6)–(8)

$$F(x) = d(x) - (\varepsilon_{\mathrm{CoTMPyP}} - \varepsilon_{\mathrm{CoTPPS}})x - \varepsilon_{\mathrm{CoTPPS}} \quad (6)$$

$$d(x) = A_r/(C_{\mathrm{CoTMPyP}} + C_{\mathrm{CoTPPS}}) \quad (7)$$

$$x = C_{\mathrm{CoTPPS}}/(C_{\mathrm{CoTMPyP}} + C_{\mathrm{CoTPPS}}) \quad (8)$$

where $\varepsilon_{\mathrm{CoTMPyP}}$ and $\varepsilon_{\mathrm{CoTPPS}}$ are the molar absorption coefficients of CoTMPyP and CoTPPS, respectively, and C is the molar concentration. This method is based on the fact that the absorbance corresponds to the sum of the absorbances of the product and reactant. The Job plots of Co(II)TMPyP and Co(II)TPPS show the lowest $F(x)$ at the 1:1 equivalence point (Fig. 4a). These results support the idea that the dinuclear cobalt porphyrin is formed by the interaction between each porphyrin ring during aggregation in DMSO. The Job plots do not show a sharp V shape. The curve at the 1:1 equivalence point suggests a dissociation equilibrium of the dinuclear porphyrin according to eqn. (9). $F(x)$ describes the dissociation constant K_d as in eqns. (11)–(14).

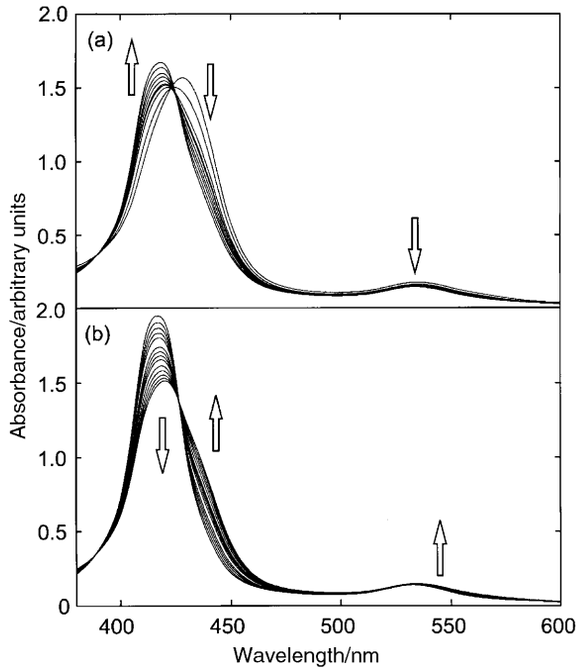

Fig. 3 Change in electronic absorption spectra upon titration of an ionic cobalt porphyrin in DMSO. The initial concentration of complex porphyrin was 10 mM: (a) Titration of Co(II)TMPyP with Co(II)TPPS (end ratio = 1 : 1), (b) titration of Co(II)TPPS with Co(II)TMPyP (end ratio = 1 : 1).

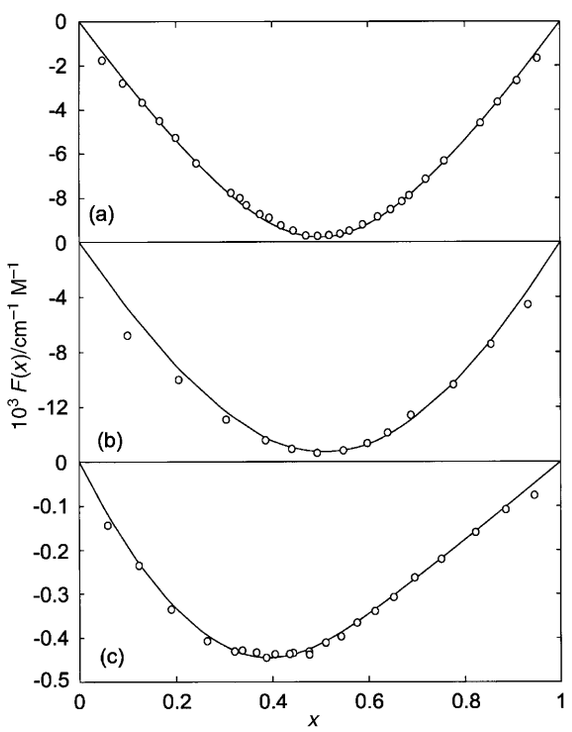

Fig. 4 Job plots of the spectroscopic change against molar ratio of CoTPPS: (a) Co(II)TPPS–Co(II)TMPyP at 420 nm, (b) Co(III)TPPS–Co(II)TMPyP at 428 nm and (c) Co(III)TPPS–Co(III)TMPyP at 566 nm. $F(x) = \varepsilon\{B - [B - 4C^2(1 - x)x]^{1/2}\}/2C$.

$$\text{Co(II)TMPyP–Co(II)TPPS} \rightleftharpoons \text{Co(II)TMPyP} + \text{Co(II)TPPS} \quad (9)$$

$$K_d = [\text{CoTMPyP}][\text{CoTPPS}]/[\text{CoTMPyP–CoTPPS}] \quad (10)$$

$$F(x) = \varepsilon\{B - [B - 4C^2(1 - x)x]^{1/2}\}/2C \quad (11)$$

$$\varepsilon = \varepsilon_{\text{Co(II)TMPyP–Co(II)TPPS}} - (\varepsilon_{\text{Co(II)TMPyP}} - \varepsilon_{\text{Co(II)TPPS}}) \quad (12)$$

Table 1 Dimerization equilibrium and kinetic properties of the TPPS–TMPyP mixed system in DMSO

Porphyrin	$10^6 K_d/M^1$	$10^{-3} k_t/M^{-1} s^{-1}$
Co(II)TPPS–Co(II)TMPyP	1.3	4.2
Co(III)TPPS–Co(II)TMPyP	2.5	2.3
Co(III)TPPS–Co(III)TMPyP	5.0	1.0
Co(II)TPPS–H_2TMPyP	0.83	8.2
H_2TPPS–Co(II)TMPyP	1.0	[a]
H_2TPPS–H_2TMPyP	0.67	[a]

[a] Too fast to measure.

$$C = C_{\text{Co(II)TMPyP}} + C_{\text{Co(II)TPPS}} \quad (13)$$

$$B = C + K_d \quad (14)$$

K_d was determined by curve fitting (the theoretical one being shown as a solid line) as 1.3×10^{-6} M for the cobalt(II) porphyrin. This result means at 0.1 mM concentration the dinuclear form is at a level of 89% in DMSO under equilibrium conditions. Similar Job plots were observed during the titration of the cobalt(II) porphyrins with the metal free porphyrins and with cobalt(III) porphyrins. These results are summarized in Table 1. The plots indicate the formation of dinuclear porphyrins except for the Co^{III}–Co^{III} system. The K_d value is influenced by the valence of the cobalt porphyrin. Increasing the valence from II to III leads to an increase in K_d due to the ionic charge repulsion. Also the coordination ability of the trivalent cobalt complex with axial ligands is larger than that of the divalent one. The DMSO solvent is strongly coordinated to the cobalt(III) porphyrin, which promotes dissociation.

Aggregation to give a trivalent cobalt porphyrin takes place in DMSO due to its strong hydrophobocity. In the trivalent system, the Job plots do not show a minimum at the 1 : 1 ratio, the monitoring wavelength being 566 nm (Fig. 4c). The ratio at the minimum is 0.33 : 1. This means that a trinuclear species (CoTPPS–CoTMPyP–CoTPPS) was also formed in the solution in addition to the dinuclear. However its degree of formation was negligibly small at a 1 : 1 ratio (CoTPPS : CoTMPyP). The Job plot coincides with the theoretical one based on the formation of trinuclear and dinuclear species. The formation of the former is electrostatically favorable due to the decrease in total charge of the complex according to eqns. (15)–(17). However, its formation constant ($K_t = 2 \times 10^3$ M^{-1})

$$[\text{Co(III)TPPS}]^{3-} + [\text{Co(III)TMPyP}]^{5+} \rightleftharpoons [\text{Co(III)TPPS–Co(III)TMPyP}]^{2+} \quad (15)$$

$$[\text{Co(III)TPPS–Co(III)TMPyP}]^{2+} + [\text{Co(III)TPPS}]^{3-} \rightleftharpoons [\text{Co(III)TPPS–Co(III)TMPyP–Co(III)TPPS}]^{-} \quad (16)$$

$$K_t = \frac{[\text{Co(III)TPPS–Co(III)TMPyP–Co(III)TPPS}]}{[\text{Co(III)TPPS}][\text{Co(III)TPPS–Co(III)TMPyP}]} \quad (17)$$

is much lower than that of the dinuclear complex (K_d^{-1}) due to the hindrance of DMSO which is more strongly coordinated with CoTMPyP than CoTPPS.

Solvent coordination inhibits formation of the dinuclear complex. K_d increases with an increase in the number of metal ions (Co–Co > Co–H_2P > H_2P–H_2P); the metal-free diporphyrin has the smallest K_d value.

The rate of formation of the dinuclear species when CoTMPyP was added to a solution of CoTPPS was spectrophotometrically measured by monitoring the absorbance of the mixture at 421 nm as a function of time. A typical time course of $F(x)$ as defined in the Experimental section is shown in Fig. 5, which was analysed based on the kinetics of a 2nd order equilibrium reaction. The rate constant obtained from the slope

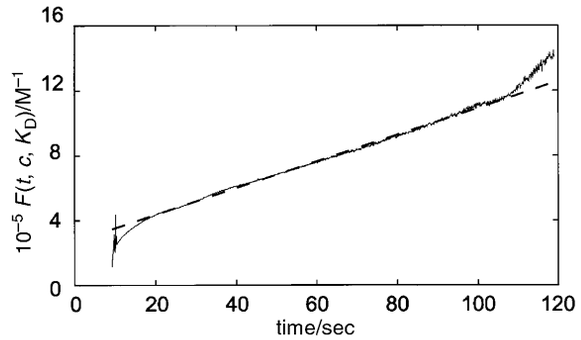

Fig. 5 Kinetic plot of the data from a time-course measurement of the absorbance for the "dimerization" of Co(II)TPPS with H_2TMPyP in order to determine the dimerization rate constant.

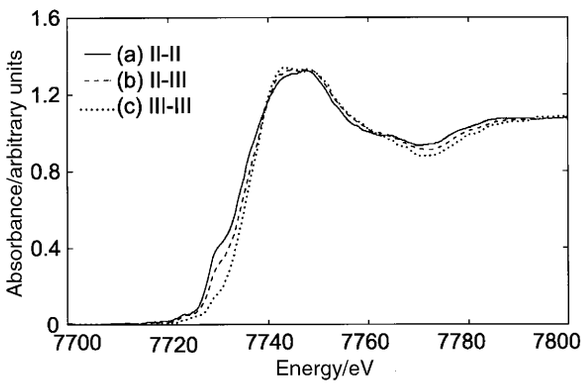

Fig. 6 The cobalt K-edge XANES spectra of the dinuclear cobalt porphyrins with change in metal valence state: (a) II–II, (b) II–III and (c) III–III.

of the plot in Fig. 5 is 8.2×10^3 M^{-1} s^{-1}, which means that for concentrations in the micromolar range a few minutes are required to attain equilibrium. It follows that the electrochemical responses shown in Fig. 1(c)–1(e) represent snapshots of the species present in solution that were influenced by the slow response of the equilibrium to an electrochemically induced concentration change near the electrode surface.

The formation rate of the dinuclear cobalt porphyrin decreases with increasing K_d of the porphyrin (Table 1). For the metal-free porphyrin the spectrophotometric method did not allow us to determine the precise constant due to too fast a reaction. This result also supports the idea that the coordination of DMSO retards the "dimerization". The "dimerization" of ionic porphyrins such as H_2TmPyP and Co(II)TPPS attains equilibrium within the order of a minute. The kinetics of the dissociation allows us to snapshot the species present without perturbing the equilibrium distribution. The 2-electron transfer process of the dinuclear porphyrin was observed by cyclic voltammetry.

The cobalt K-edge XANES spectra of the dinuclear cobalt porphyrins are shown in Fig. 6 where the K-edge is shifted to a higher energy, *ca.* 3 eV, with increasing valence. Divalent (II–II and II–III) dinuclear porphyrins show a shoulder peak at 7.728 keV, which is similar to that of previously reported divalent cobalt complexes.[42]

The distance between cobalt centres in the dinuclear porphyrins was measured by EXAFS. Fourier transform of the original EXAFS spectra was performed after extracting the EXAFS vibrations (Fig. 7). In Table 2 the Co–N and Co–Co distances are summarized. The Co–N distance in Co(II)TPPS–Co(II)TMPyP is estimated to be 1.96 Å, similar to the value previously reported for Co(TPP) based on a crystallographic analysis (1.949 Å).[43] The Co···Co distance was determined to be 3.37 Å. This distance was not significantly influenced by the valence state because the porphyrin is strongly fixed by four ionic groups. Therefore, it coincides with the most stable

Table 2 EXAFS atom–atom distance data for dinuclear cobalt porphyrins

Porphyrin	Co···Co Å	Co–N Å
Co(II)TPPS–Co(II)TMPyP	3.37	1.962
Co(III)TPPS–Co(II)TMPyP	3.36	1.942
Co(III)TPPS–Co(III)TMPyP	3.37	1.927

Table 3 Quantitative UV-vis spectra of porphyrins in DMSO

Porphyrin	λ_{max}/nm ($10^{-5}\varepsilon$/M^{-1} cm^{-1}	
H_2TPPS	420 (5.15)	516, 551, 591, 647
H_2TMPyP	425 (2.66)	516, 549, 589, 644
Co(II)TPPS	416 (1.96)	533 (0.15)
Co(III)TPPS	435 (2.85)	548 (0.18)
Co(II)TMPyP	428 (1.57)	536 (0.17)
Co(III)TMPyP	441 (1.59)	553 (0.18)
Co(II)TPPS–Co(II)TMPyP	420 (2.99)	534 (0.27)
Co(III)TPPS–Co(II)TMPyP	435 (3.22)	545 (0.25)
Co(III)TPPS–Co(III)TMPyP	436 (4.39)	548 (0.30)
Co(II)TPPS–H_2TMPyP	423 (2.77)	518, 546,[a] 589, 643
Co(III)TPPS–H_2TMPyP	430 (2.66)	516, 545, 588, 643
H_2TPPS–Co(II)TMPyP	420 (5.74)	516, 549, 589,[a] 645
H_2TPPS–Co(III)TMPyP	420 (5.44)	517, 548, 591, 646

[a] Shoulder peak.

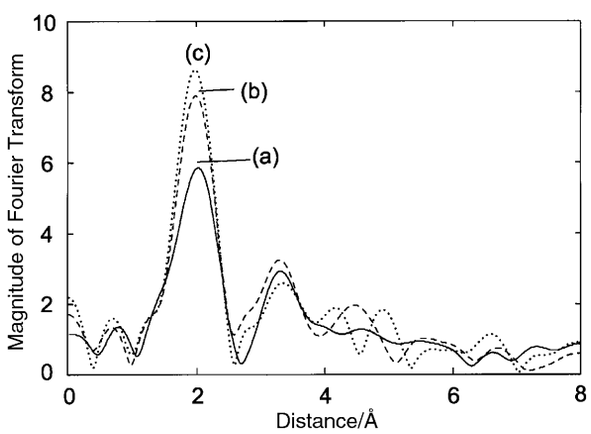

Fig. 7 Variations of the Fourier transforms of the EXAFS spectra $k^3\chi(k)$ for the dinuclear cobalt porphyrins with valence state: (a) II–II, (b) II–III and (c) III–III.

distance based on π–π stacking of the porphyrin rings, and is similar to that of a previously reported dinuclear porphyrin (3.42 Å) linked by amide bonds.[44] This result indicates that the resulting dinuclear species maintains a co-facial structure.

On the basis of the K_d of Co(II)TPPS–Co(II)TMPyP, only *ca.* 60% of the complex exists as the dinuclear species in a 1×10^{-5} M DMSO solution. Our prepared ultra-thin layer cell allowed us to measure the spectra at a high concentration of the complex in which the ratio of the dinuclear species remains high in the mixture (>90%). The spectroelectrochemical data are summarized in Table 3. The resulting spectra do not agree with the sums of those of the individual reagents. The spectra changed with the applied potential, having two isosbestic points (426.6, 540.5 nm). These changed to 428.3 and 539.2 nm with potentials between −0.6 and 0 V (*vs.* Fc–Fc^+). The 2-step electron transfer processes correspond to the oxidation of Co^{II}–Co^{II} to Co^{II}–Co^{III} and Co^{II}–Co^{III} to Co^{III}–Co^{III}. These results indicate the formation of a mixed valence state in the dinuclear complex, which is also supported by cyclic voltammetry. Red shifts in the Soret and Q band were observed during oxidation of the dincuclear complex from the II–II to the II–III valence state as well as of the monomeric cobalt porphyrin,

Table 4 Redox potentials of "dimeric" cobalt porphyrins[a]

Porphyrin	$E_{1/2}$/V *vs.* Fc–Fc^{+} [b]	
	Co(II/III)TPPS	Co(II/III)TMPyP
CoTPPS	−0.33[c]	
CoTMPyP		−0.21
CoTPPS–H_2TMPyP	−0.37	
H_2TPPS–CoTMPyP		−0.16
CoTPPS–CoTMPyP	−0.37	−0.17

[a] From cyclic voltammograms at a platinum electrode measured at 10 mV s^{-1} in N_2 saturated DMSO–0.05 M NBu_4ClO_4. [b] $E_{1/2} = ½(E_{Pa} + E_{Pc})$. [c] Including 5 wt% CF_3CO_2H.

which is based on a decrease in the band gap between a_{2u}, $a_{1u}(\pi)$ and $e_g(\pi^*)$ due to a reduction in the energy level of e_g* through electron transfer at the d_{z^2} orbital.

The decrease in the absorbances of the Soret and Q bands indicates π stacking of the porphyrin rings, even though the λ_{max} changes are only 1 nm. A large shift in λ_{max} and/or new peaks were not observed upon "dimerization". The "dimeric" porphyrins having only one cobalt nucleus also showed similar behavior in which the absorbances of the Soret and Q bands decrease in comparison with the sum of each reagent spectrum in spite of no large shift in the λ_{max} value (Fig. 2b, 2c). Both CoTMPyP–H_2TPPS and CoTPPS–H_2TMPyP also possess a π–π interaction.

Cyclic voltammetry provides useful information about the valence in this system even though the equilibrium of the dissociation changes during the electron transfer because its rate is relatively low so that typical electrochemical measurements provide snapshots of the species present without perturbing this equilibrium distribution. Therefore, cyclic voltammetry was performed in order to obtain the electrochemical response of the dinuclear species (0.1 mM). The redox potentials of the cobalt porphyrins are summarized in Table 4. Two redox waves were observed at −0.37 and −0.17 V *vs.* Fc–Fc^{+}(Fig. 1e) in the cyclic voltammogram, which is definitely different from that of monomeric cobalt porphyrins (Co(II)TPPS, −0.33; Co(II)-TMPyP: −0.21 V). The redox couples are ascribed to Co^{II}–Co^{II}/Co^{II}–Co^{III} and Co^{II}–Co^{III}/Co^{III}–Co^{III} on the basis of the spectroelectrochemical data (Fig. 2e–2g).

The cyclic voltammogram was compared to those for the "dimeric" porphyrins with only one cobalt center which present a more accurate electronic structure than the monomeric ones as model compounds. Thus Co(II)TPPS–H_2TMPyP and Co(II)TMPyP–H_2TPPS show redox potentials at −0.37 and −0.16 V (Fig. 1c,d), respectively. The redox potentials are in good agreement with those of the dinuclear cobalt porphyrins. Each cobalt center in the latter does not electrochemically interact through electron transfer in spite of the overlapping π orbitals of the porphyrin rings. In the II–III valence state an intervalence transition band was not observed in near IR region These results indicate no interaction between the metal centers in the dinuclear cobalt porphyrins because the potential curve for the electron transfer is asymmetrical with low activation barriers.[45]

The redox potentials of Co(II)TPPS and Co(II)TMPyP are shifted to a more negative potential and positive one, respectively, in comparison with those of the dinuclear species. This means that the d_{z^2} orbital on cobalt interacts with the π orbital of the porphyrin on the co-facial porphyrin ring. That is, these shifts *versus* the monomeric porphyrin are caused by an electronic effect due to π–π stacking.

The catalytic behavior of the dinuclear cobalt porphyrin complexes was studied using an electrochemical method with a modified glassy carbon electrode. However, the complex could not stably be adsorbed on the glassy carbon electrode for electrochemical measurements in an acidic atmosphere. Poly-

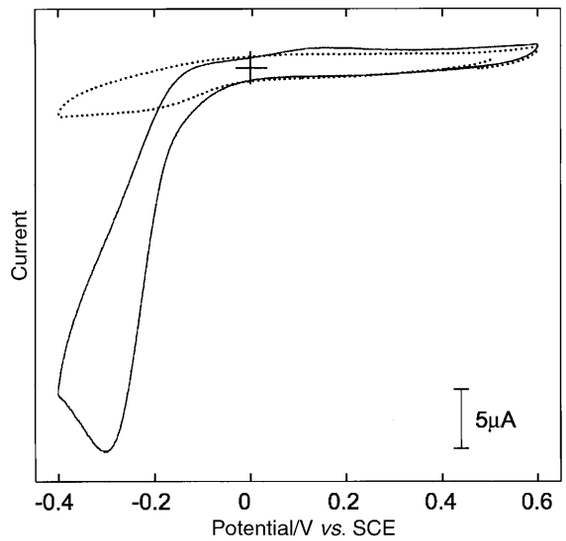

Fig. 8 Cyclic voltammograms showing reduction of O_2 at a glassy carbon electrode modified by the poly(2,3-dicarboxyaniline)–Co(II)-TMPyP–Co(II)TPPS complex under an air atmosphere. The dotted line shows the voltammogram in an argon atmosphere. Supporting electrolyte: 0.1 M KPF_6 aqueous solution (pH 6.15).

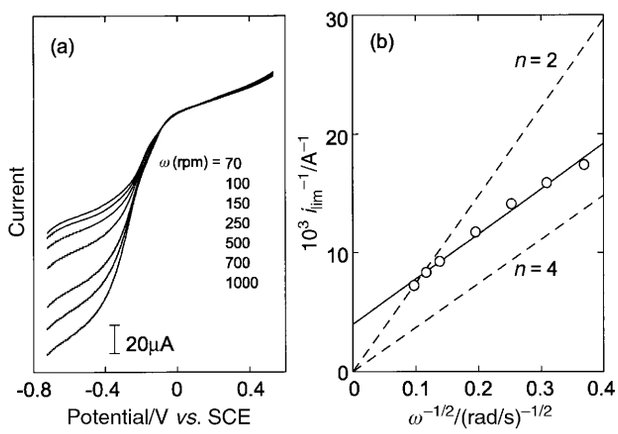

Fig. 9 (a) Rotating disk voltammetry showing reduction of O_2 at a glassy carbon electrode modified by poly(2,3-dicarboxyaniline)–Co(II)MTMPyP–Co(II)TPPS complex. Supporting electrolyte as in Fig. 8. Rotation rates (ω/rpm) are listed. (b) Koutecky–Levich plots of the plateau current obtained (○). The dashed lines are calculated plots for 2- and 4-electron reductions of oxygen.

(dicarboxyaniline) was used as the conductive matrix to hold the cobalt porphyrin. The polymer complex allows stable electrochemical responses. Fig. 8, shows a typical cyclic voltammogram measured at a glassy carbon electrode in an N_2 saturated aqueous solution. When the electrode was transferred to an oxygen saturated solution a large catalytic current appeared at $E_c^{1/2}$ = *ca.* −0.2 V *vs.* SCE. The half-wave potential of the reduction of oxygen was shifted to anodic value at 0.15 V at pH 0.4 in the presence of perchloric acid. The direct reduction of O_2 to H_2O_2 on an uncoated portion of the carbon electrode is observed at a less anodic potential near −0.5 to −0.75 V.

Quantitative kinetic data for the electro-reduction of oxygen by the dinuclear cobalt porphyrin were obtained using rotating disk voltammetry (Fig. 9a). A controlled experiment using a monomeric cobalt porphyrin modified electrode showed a slope of 2 ± 0.2 for the electron transfer reaction in the Koutecky–Levich plot.[46,47] For the polyaniline–dinuclear complex the Koutecky–Levich plot of the plateau current became linear. The slope matches the *n* value (number of electrons transferred) of 3.9 ± 0.1, which means that the dinuclear cobalt porphyrin with ionic groups acts as an excellent catalyst for the four-electron reduction of oxygen to water in the polyaniline

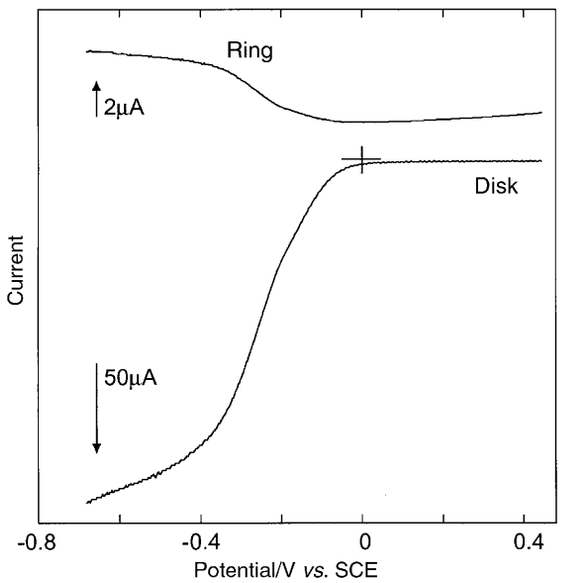

Fig. 10 Rotating ring and disk voltammetry showing reduction of O_2 at a glassy carbon electrode modified by poly(2,3-dicarboxyaniline)–Co(II)TMPyP–Co(II)TPPS. Supporting electrolyte as in Fig. 8. Rotation rate 1500 rpm. The disk potential was scanned at 20 mV s^{-1}. The ring electrode was maintained at 1.0 V *vs*. SCE.

(Fig. 9b). These results are also confirmed by the electrochemical detection of H_2O_2 as a side-product at a ring-disk electrode. The voltammograms were obtained with a rotating platinum ring glassy carbon disk electrode under the same conditions, with an applied potential of 1.0 V to detect the H_2O_2 generated by the reduction of oxygen as a side reaction at the disk electrode. A comparison of the resulting collection efficiency with the theoretical one ($N_o = 0.39$)[48] revealed the selectivity of the 4-electron transfer during the electro-reduction of oxygen. Controlled experiments using the monomeric cobalt porphyrin modified electrode show a 93 ± 5% formation of H_2O_2 through a 2-electron transfer reaction in pH 4.5 buffer solution. The rotating ring disk voltammetry (RRDV) at the dinuclear cobalt porphyrin polymer complex-modified electrode results in the reduction of more than 85% of the oxygen molecules to water (Fig. 10). The selectivity of the 4-electron pathway is in good agreement with the *n* value determined from the Koutecky–Levich plots. The potential of the easy-to-prepare component promises to expand the wide range of application of this catalyst.

Conclusion

The dinuclear cobalt porphyrin undergoes a 2-step electron transfer accompanied by a dissociation equilibrium (Scheme 1).

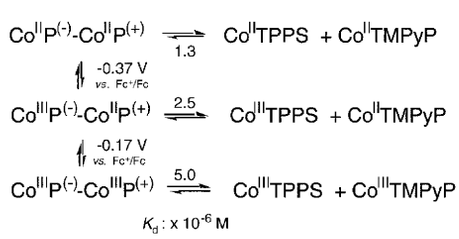

Scheme 1 Two-electron transfer system of the dinuclear cobalt porphyrin accompanied by a dissociation equilibrium.

The dissociation constants for each valence state were determined to be 1.3×10^{-6}, 2.5×10^{-6} and 5.0×10^{-6} M using Job plots for the monomeric cobalt porphyrin in each valence state. The K_d value increases with an increasing valence due to charging. The reactions of Scheme 1, which control the equilibriums, showed a kinetic time scale in the order of a minute. This means that the 2-electron transfer process of the dinuclear porphyrin dominates the chemistry. In the present study we have observed a catalytic efficiency up to 95% for the 4-electron reduction of oxygen to water using a glassy carbon electrode modified by a polymer complex of the dinuclear porphyrin. Also, our results revealed that this reduction could be achieved under pseudo-neutral conditions (0.1 M KPF_6 aqueous solution, pH 6.2). However, monomeric cobalt porphyrin or polyaniline only results in a 2-electron reduction.

Acknowledgements

This work was partially supported by Grants-in-Aid for Scientific Research (Nos. 11555253, 1265087, 12023246, 11167273) from the Ministry of Education, Science, Sports, and Culture, Japan, Grant-in-Aid for the Development of Innovative Technology (No. 12407) from the Science and Technology Agency, and a Kanagawa Academy of Science and Technology Research Grant.

References

1 J. H. Fuhrhop, *Angew. Chem., Int. Ed. Engl.*, 1976, **15**, 648.
2 H. Song, C. A. Reed and W. R. Scheidt, *J. Am. Chem. Soc.*, 1989, **111**, 6865.
3 S. Iwata, C. Ostermeier, B. Ludwig and H. Michel, *Nature* (*London*), 1995, **376**, 660.
4 T. Tukihara, H. Aoyama, E. Yamashita, T. Tomizuka, H. Yamaguchi, K. Itoh, R. Nakashima, R. Yaono and S. Yoshikawa, *Science*, 1995, **269**, 1069.
5 G. Shalla and J. Reedijk, *Macromol. Chem. Macromol. Symp.*, 1992, **59**, 59.
6 K. Yamamoto, E. Shouji, S. Kobayashi and E. Tsuchida, *J. Org. Chem.*, 1996, **61**, 1912.
7 J.-E. Backvall, R. B. Hopkins, H. Grennberg, M. M. Mader and A. K. Awasthi, *J. Am. Chem. Soc.*, 1990, **112**, 5160.
8 H. Grennberg, S. Faizon and J.-E. Backvall, *Angew. Chem., Int. Ed. Engl.,* 1993, **32**, 263.
9 M. S. Nasir, B. I. Cohen and K. D. Karlin, *J. Am. Chem. Soc.*, 1992, **114**, 2482.
10 B. Steiger and F. C. Anson, *Inorg. Chem.*, 1997, **36**, 4138.
11 C. Shi, B. Steiger, M. Yuasa and F. C. Anson, *Inorg. Chem.*, 1997, **36**, 4294.
12 C. Shi and F. C. Anson, *Inorg. Chem.*, 1998, **37**, 1037.
13 R. Karaman, S. Jeon, O. Almarsson and T. C. Bruice, *J. Am. Chem. Soc.*, 1992, **114**, 4899.
14 J. P. Collman, P. Denisevich, Y. Konai, M. Marrocco, C. Koval and F. C. Anson, *J. Am. Chem. Soc.*, 1980, **102**, 6027.
15 K. Yamamoto, K. Oyaizu and E. Tsuchida, *J. Am. Chem. Soc.*, 1996, **118**, 12665.
16 K. Yamamoto and D. Taneichi, *Chem. Lett.*, 2000, 4.
17 K. Yamamoto, S. Nakazawa and A. Matsufuji, *Mol. Cryst. Liq. Cryst.*, 2000, **342**, 255.
18 C. Endisch, J.-H. Fuhrhop, J. Buschmann, P. Luger and U. Siggel, *J. Am. Chem. Soc.*, 1996, **118**, 6671.
19 L. Ruhlmann, A. Nakamura, J. G. Vos and J.-H. Fuhrhop, *Inorg. Chem.*, 1998, **37**, 6052.
20 T. Sawaguchi, T. Matsue, K. Itaya and I. Uchida, *Electrochim. Acta*, 1991, **36**, 703.
21 T. Fournier, Z. Liu, T. Tran-Thi, T. D. Houde, N. Brasseur, C. L. Madeleine, R. Langlois, J. E. V. Lier and D. Lexa, *J. Phys. Chem. A*, 1999, **103**, 1179.
22 F. D'Souza, Y.-Y. Hsieh and G. R. Deviprasad, *Chem. Commun.*, 1998, 1027.
23 G. C. Allen and N. S. Hush, *Prog. Inorg. Chem.*, 1967, **8**, 357.
24 P. Ceroni, F. Paolucci, C. Paradisi, A. Juris, S. Roffia, S. Serroni, S. Campagna and S. A. J. Bard, *J. Am. Chem. Soc.*, 1998, **120**, 5480.
25 C. Patoux, J.-P. Launay, M. Beley, S. Chodorowski-Kimmes, J.-P. Collin, S. James and J.-P. Sauvage, *J. Am. Chem. Soc.*, 1998, **120**, 3717.
26 T.-Y. Liu, Y. J. Chen, C.–C. Tai and K. S. Kwan, *Inorg. Chem.*, 1999, **38**, 674.
27 D. O. Cowan, C. LeVanda, J. Park and F. Kaufman, *Acc. Chem. Res.*, 1973, **6**, 1.
28 M. Yasuda, T. Nagaiwa, M. Kato, I. Sekine and S. Hayasi, *J. Electrochem. Soc.*, 1995, **142**, 2612.
29 R. F. Pasternack, *Inorg. Chem.*, 1985, **24**, 3777.

30 R. J. H. Chan, Y. O. Su and T. Kuwana, *Inorg. Chem.*, 1985, **24**, 3777.
31 J. A. Bolfo, T. D. Smith, J. F. Boas and J. R. Pilbrow, *J. Chem. Soc., Dalton Trans.*, 1976, 1495.
32 O. Ikeda, K. Okabayashi, N. Yoshida and H. Tamura, *J. Electroanal. Chem. Interfacial Electrochem.*, 1985, **191**, 15.
33 P. Neta, *J. Phys. Chem.*, 1981, **85**, 3678.
34 K. Yamamoto and D. Taneichi, *Macromol. Chem. Phys.*, 2000, **201**, 6.
35 H. Segawa, H. Nishino, T. Kamikawa, K. Honda and T. Shimidzu, *Chem. Lett.*, 1989, 1917.
36 K. Yamamoto and S. Nakazawa, *Chem. Lett.*, 2000, 225.
37 D. Pang and Z. Wang, *J. Electroanal. Chem. Interfacial Electrochem.*, 1993, **358**, 235.
38 C. Araullo-McAdams and K. M. Kadish, *Inorg. Chem.*, 1990, **29**, 2749.
39 J. F. Lipskier and T. H. Tran-Thi, *Inorg. Chem.*, 1993, **32**, 722.
40 P. Job, *Ann. Chim.*, 1928, **9**, 113.
41 Z. D. Hill and P. MacCarthy, *J. Chem. Educ.*, 1986, **63**, 162.
42 T. Akai, M. Okuda, K. Horiuchi, J. Matsuura, Y. Koike, M. Yimagawa and T. Fujikawa, *Jpn. J. Appl. Phys.*, 1994, **33**, 6360.
43 P. Madura and W. R. Scheidt, *Inorg. Chem.*, 1976, **15**, 3182.
44 J. P. Collman, P. S. Wagenknecht and J. E. Hutchison, *Angew. Chem., Int. Ed. Engl.*, 1994, **33**, 1537.
45 T. Ito, T. H. Hamaguchi, H. Nagino, T. Yamaguchi, J. Washington and C. P. Kubiak, *Science*, 1997, **277**, 660.
46 C. Shi and F. C. Anson, *J. Am. Chem. Soc.*, 1991, **113**, 9564.
47 C. Shi and F. C. Anson, *Inorg. Chem.*, 1992, **31**, 5078.
48 The theoretical collection efficiency of the ring disk electrode was determined to be $N_o = 0.39$ in an independent experiment with 0.1 mM of $K_3[Fe(CN)_6]$ in pH 4.5 buffer solution. The normalization of the collection efficiency $[(N_0 - N)/(N_o + N)]$ used the ratio of the ring-disk to disk currents.